ORIGINAL PAPER

Comparison of shock-buffet dynamics on a supercritical airfoil with and without a pitching degree of freedom

Sven Scharnowski[1] · Alessandro Accorinti[1] · Tim Korthäuer[1] · Christian J. Kähler[1]

Abstract

With the goal of understanding the dynamics of the transonic flow around an OAT15A airfoil model, velocity field measurements were performed by means of high repetition rate particle image velocimetry. The experiments were performed at free-stream Mach numbers from 0.70 to 0.77 and at a Reynolds number of $\mathrm{Re_c} \approx 3 \times 10^6$. The variation of the Mach number allowed for an investigation in the pre-buffet, buffet and close to buffet-offset regime. A fixed version and a spring mounted version of the model were used to investigate the effect of the pitching degree of freedom on the shock buffet. The dominant structural frequency of the airfoil's pitch motion was adjusted to be in the range of the natural buffet frequency of the flow with inhibited pitching motion of the model. Flow field measurements with an acquisition rate of 4 kHz allowed for the detection and analysis of the shape and the motion of the compression shock. With released pitching degree of freedom, shock buffet started at a lower Mach number and showed a larger amplitude for the shock oscillation. Furthermore, the shock motion appeared more harmonic compared to the model without pitching degree of freedom. For a Mach number of $M_\infty = 0.72$ and 0.74, the change of the angle of attack and the shock location correlated strongly with each other. From the measurements, the phase lag between both quantities during the coupled motion could be determined. From the correlation of the shock position at different heights, it can be concluded that the shock motion is controlled by events at the shock foot. The movement of the upper shock part is only a reaction to the movement of the lower part.

Keywords Transonic buffeting · Experimental aero-elasticity · Fluid–structure interaction

1 Introduction

If the transonic flow over an airfoil accelerates to supersonic speed, the supersonic region is terminated by means of a compression shock. The pressure rises abruptly and the velocity drops accordingly due to the shock. Depending on the shock strength and the state of the boundary layer, separation can occur due to the sudden increase in pressure. For a certain range of inflow Mach numbers and angles of attack, there is no stable solution for the shock position and the boundary layer state depending on the airfoil geometry.

In this range, the shock executes a periodic motion coupled with a shock-induced separation of the boundary layer, known as shock-buffet [1–7]. The flow separation affects the flow direction downstream of the shock and causes the shock

to incline and to move upstream. The separation area starts at the shock foot and increases as the shock moves upstream. The further the shock moves towards the leading edge of the model, the lower become the pre-shock Mach number, the shock strength as well as the pressure increase across the shock. Consequently, the separation collapses and the flow follows the model contour, causing the shock to move downstream once again until separation occurs. This closes the so-called buffet cycle, as sketched in Fig. 1.

Shock-induced buffet causes strong periodic pressure fluctuations and limits the operating range of technical components like aircraft wings. The consideration of coupling between fluid and structure is particularly relevant since real structures are never infinitely stiff. Recent numerical simulations have shown that the natural frequencies of elastic structures can have an influence on the buffet frequency and on the buffet boundary [8, 9].

In order to analyze the coupling between fluid and structure, a quasi-two-dimensional airfoil model with a optional pitching degree of freedom (DOF) whose natural frequency

✉ Sven Scharnowski
sven.scharnowski@unibw.de

1   Institut für Strömungsmechanik und Aerodynamik,
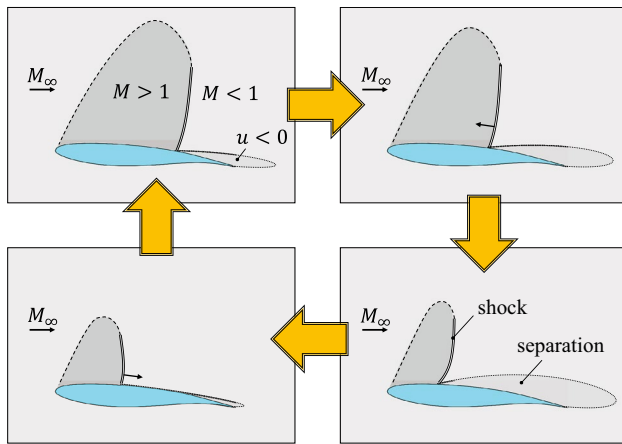   Universität der Bundeswehr München, Neubiberg, Germany

Fig. 1 Schematic diagram of the Buffet cycle with varying shock location and boundary layer state

Fig. 2 Sketch of the wind tunnel model with the essential flow features as well as the light sheet and the field of view for the PIV experiments [11]

is close to the buffet frequency is investigated in this work. The analysis outlined here is a continuation of Refs. [10, 11], in which the flow around the fixed airfoil and the airfoil with pitching degree of freedom were considered separately. In the present paper, the focus is set on the characterization of the flow field, and in particular on how the shape and motion of the compression shock change when the model is allowed to pitch at the buffet frequency.

The following section briefly describes the test facility, the wind tunnel model and the measurement approach. In Sec. 3, the measurement results are presented and discussed in detail. The work is summarized and conclusions are drawn in Sec. 4.

2 Measurement setup

The measurements were carried out in the Trisonic Wind Tunnel at the Bundeswehr University in Munich (TWM). The TWM is a blow-down wind tunnel that can be operated in the Mach number range from 0.3 to 3.0. The 300 mm wide and 675 mm high test section was specially designed for the investigation of airfoil flow. The Reynolds number in the test section is set via the total pressure, which can be varied between 1.2 and 5 bar. In Ref. [12], a turbulence level of about 1.3% was determined for the investigated Mach numbers. Further details about the facility and its characterization are given in Refs. [12, 13].

The wing model consists of upper and lower shells made of carbon fiber reinforced plastic and a steel shaft located at 25% of the chord length. This shaft extends through the side windows of the test section and is held in place by needle bearings just outside the windows. This design ensures that
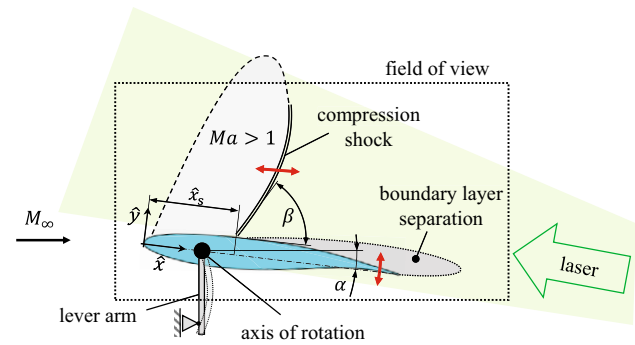
the model can rotate around the axis of the shaft, as shown in Fig. 2.

To enable the comparison between 0-DOF and 1-DOF, the model was mounted in two different ways outside the test section. For the 0-DOF case, massive lever arms were screwed onto the ends of the steel shaft, which prevent the pitching movement to a high degree. The resulting natural frequencies for bending ($\approx$ 170 Hz), pitch coupled with surge ($\approx$ 280 Hz) and pitch ($\approx$ 385 Hz) were far away from the buffet frequency ($\approx$ 100 Hz), according to Refs. [10, 14]. For the 1-DOF case, steel levers with a rectangular cross-section ($6 \times 10\,\text{mm}^2$) extend downwards from both shaft ends. These levers act as springs and their stiffness can be adjusted via the lever length. In addition, balancing masses are used to keep the center of gravity of all moving parts on the axis of rotation. This decouples the structural pitch and lift modes in wind-off conditions. The eigenfrequency of the model's pitching motion was adjusted to 105 Hz, which is about equal to the buffet frequency of the rigidly suspended airfoil. During the wind tunnel tests, the model bends slightly in the spanwise direction. The static displacement on the center of the model compared to the ends is no more than about 0.5% of the chord length. Since the spanwise bending frequency ($\approx$ 145 Hz) is far away from the buffet frequency it is not excited for the here investigated flow cases and the model is considered to be sufficiently stiff [15, 16].

The airfoil geometry was that of a supercritical airfoil OAT15A. The chord length of the model was 150 mm and the width 298 mm. As a result, there was a gap of 1 mm on each side, necessary for the pitching motion for the 1-DOF case. The aspect ratio of 2 is relatively low, so that a pure 2D flow cannot be expected. For a larger aspect ratio, a shorter model would be required. However, this would increase the relative mass of the model (and thus affect the flutter behavior) and would make it more difficult to see small scale flow structures. The aspect ratio of 2 is a reasonable compromise. The boundary layers on the side walls have a thickness of

about 30 mm [17], so that only about 10% are affected on both sides and a quasi 2D shock is formed in the center region of the span [18].

For the experiments with and without pitching degree of freedom, four different Mach numbers between $M_\infty = 0.70$ and 0.77 are investigated in this work. The Reynolds number based on the chord length was set to $\mathrm{Re}_c \approx 3.0 \times 10^6$ by adjusting the total pressure to $p_0 = 1.5$ bar. The angle of attack was set to $\alpha = 5.8°$ for the 0-DOF case. At this angle, there is a stable compression shock at the lowest Mach number, and as the Mach number increases, there is initially a strongly pronounced shock buffet, which then decreases in intensity for the highest Mach number. For the 1-DOF case, the angle of attack was set to $\alpha = 7.0°$. During the wind tunnel runs, the mean angle of attack decreases due to the static deformation under varying aerodynamic loads to values between 6.04° and 5.64°, depending on the Mach number. As before, stable shock, pronounced shock buffet, and decaying buffet were achieved by varying the Mach number. Values for the flow conditions of the different wind tunnel runs are summarized in Table 1.

Flow field measurements were performed by means planar PIV measurements in the center plane as sketched in Fig. 2. Di-Ethyl-Hexyl-Sebacat (DEHS) tracer particles were illuminated from downstream with a light sheet generated by a PIV double pulse laser (DM 150-532, by Photonics Industries Inc.) with a light sheet width of about 0.5 mm. A high speed camera (Phantom V2640, by Vision Research Inc.) equipped with a 50 mm lens (Planar T2/50, by Zeiss) acquired PIV double images, 2048×1264 pixel in size (corresponding to 280×170 mm^2), at a recording frequency of 4 kHz. 10,000 double images were analyzed for all cases. The particle image displacement was limited to 12 pixel for regions with a flow velocity of 400 m/s by setting the time separation between the double images to 4 μs.

The PIV measurement setup was optimized to capture an overview of the flow field to determine the shock location and the boundary layer state. Due to the richness of spatial and temporal dynamics in this kind of flow, resolving the small-scale features is only partially possible due to the strong velocity gradients in the shear layers [19].

3 Results and discussion

For all the investigated combinations of Mach number and angle of attack, the flow on the suction side of the airfoil forms a region of supersonic velocities that terminates with a compression shock. Depending on the set Mach number, shock buffet/buffeting may occur. Where the shock is located, what its shape is, how it moves, and how it interacts with the boundary layer flow and the model's pitch motion will be discussed in detail in this section.

3.1 Structural dynamics

The position of the model was determined from the PIV raw images. In the mid-plane, the position of the upper surface in the range from about the center to the trailing edge could be detected from the scattered light of the laser. With known magnification, the instantaneous angle of attack could be reliably determined from the recorded images by comparison to the model geometry.

For the model with pitching degree of freedom, the mean angle of attack is slightly decreased with increased Mach number. Furthermore, α fluctuates around its mean with an amplitude of up to $\Delta\alpha = \pm 1.17°$ for a Mach number of $M_\infty = 0.74$. For the highest and the lowest Mach numbers, however, the fluctuation amplitude is significantly smaller. The pitching motion is highly periodic, as can be seen from the temporal evolution as well as from the power spectral density in Fig. 3.

The dominant frequency is slightly larger than the natural frequency of the model's pitch motion (105 Hz at wind-off conditions) and increases with larger Mach number, see Table 1. The secondary peaks in the spectra around 400 Hz are attributed to natural frequencies of the external setup.

Table 1 Summary of the flow conditions together with statistical results of the airfoil dynamics and the shock dynamics for the different wind tunnel runs without (top) and with (bottom) pitching degree of freedom

Ma	Re$_c$	$\bar{\alpha} \pm \Delta\alpha$	f_α	$f_{\hat{x}_s}$	$k_{\hat{x}_s}$	$\tau_{max} \cdot f_\alpha$
0.70	2.93×10^6	5.8°	–	–	–	–
0.72	2.98×10^6	5.8°	–	–	–	–
0.74	3.03×10^6	5.8°	–	98.5 Hz	0.20	–
0.77	3.09×10^6	5.8°	–	≈ 120 Hz	0.23	–
0.70	2.96×10^6	6.04° ± 0.28°	108.6 Hz	–	–	–
0.72	3.01×10^6	5.91° ± 0.96°	113.3 Hz	113.3 Hz	0.229	12%
0.74	3.06×10^6	5.76° ± 1.17°	115.4 Hz	115.5 Hz	0.228	17%
0.77	3.11×10^6	5.64° ± 0.45°	118.2 Hz	123.8 Hz	0.235	–

The dimensionless frequency of the shock motion is computed using $k_{\hat{x}_s} = \pi f_{\hat{x}_s} c / u_\infty$ and τ_{max} is the phase difference between shock-foot motion and angle of attack
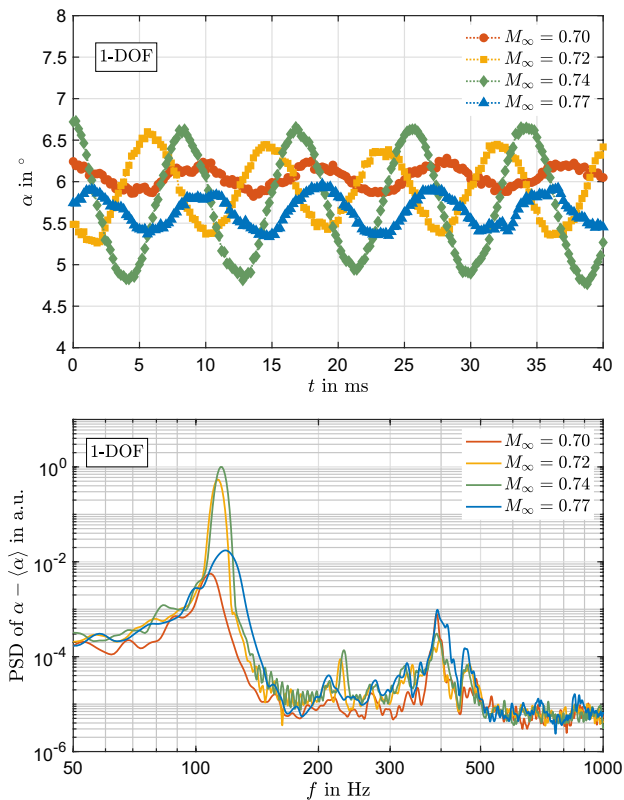
Fig. 3 Temporal evolution (top) and power spectral density (bottom) of the angle of attack α for the investigated Mach numbers in the case of the model with pitching degree of freedom

3.2 Shock detection

To determine reliable velocity fields, the PIV images were evaluated using an iterative approach with decreasing interrogation window size and subsequent image deformation. A Gaussian window weighting function was applied and a final interrogation window size of 24^2 pixel with 50% overlap was used, leading to a vector grid spacing of 1.6 mm corresponding to 1.1% of the chord length c. Invalid vectors were identified and removed with the method of Ref. [20]. For most time steps, the fraction of invalid vectors was well below 1%. Figure 4 shows exemplary velocity fields in buffet conditions for the cases without and with pitching degree of freedom. For both cases, examples of the extreme shock positions are shown. The shock was identified from the strongest gradient $\partial u/\partial x$. The shock location could be measured down to appr. $0.03\,c$ above the surface. From the points below $y/c = 0.2$, the shock-foot location on the surface was estimated by applying a second-order polynomial fit function. For better visibility, the measured shock location is illustrated by a solid line in the figure. In addition, the open circles show the extrapolated shock-foot location on the airfoil's surface.

3.3 Shock statistics

For $M_\infty = 0.74$, the shock position varies over a wide range, as can be seen in Fig. 4. The shock movement is accompanied by a change in the state of the boundary layer, which varies between attached and detached. The flow field examples in Fig. 4 show extreme upstream and downstream shock locations for times just before separation occurs and just before separated region collapses again. The flow topology for the 0-DOF case and the 1-DOF case is similar for the examples shown in the figure. It is worth mentioning that the back-flow region is more pronounced in the 1-DOF case and the shock location covers a larger range in streamwise direction. This is not only true for the example shown, but is representative for the entire time series, as can be seen for a section over 100 ms in Fig. 5. This figure shows the time evolution of the horizontal velocity component for a fixed height of $\hat{y} = 0.1$ above the chord. At this height, the 0-DOF case almost never shows reverse flow. The 1-DOF case, on the other hand, always shows a flow separation during the upstream movement of the shock, though the strength of this separation varies. Comparing the two cases in Fig. 5, it is also noticeable that the shock moves differently: in the 1-DOF case, the motion has a periodic pattern and the turning points are approximately at the same x–position. For the 0-DOF case, the shock motion appears less regular and turning points can be found at any x-position between the extreme values.

The flow fields of $M_\infty = 0.74$ show the strongest shock fluctuations, as can be seen from the comparison of the histograms in Fig. 6. For the smallest Mach number $M_\infty = 0.70$, the mean shock location and its variation are approximately equal for the cases with and without pitching degree of freedom. At $M_\infty = 0.72$, however, the two distributions are very different. While in the 0-DOF case, the fluctuation around a position further downstream is in the same range as for $M_\infty = 0.70$, the histogram broadens considerably in the 1-DOF case, indicating the onset of buffet. For $M_\infty = 0.74$, shock buffet is evident for both cases, independent from the degree of freedom. The histogram for the 0-DOF case is now also broadened, but still shows the highest probability for central shock locations. In contrast, for the 1-DOF case, the probability of finding the shock at a middle position is lower than for the turning points, as expected from the evolution of the velocity shown in Fig. 5. The histogram shows two peaks at $\hat{x}_s/c \approx 0.24$ and 0.46 and a local minimum in between. Interestingly, D'Aguanno et al. [21] observed a comparable distribution for the shock location in buffet conditions with a 0-DOF model at slightly lower Mach number and angle of attack. This is in contrast to the here presented statistics, indicating that the findings are sensitive to the test facility and the model characteristics. It is possible that in the 0-DOF cases presented here, the
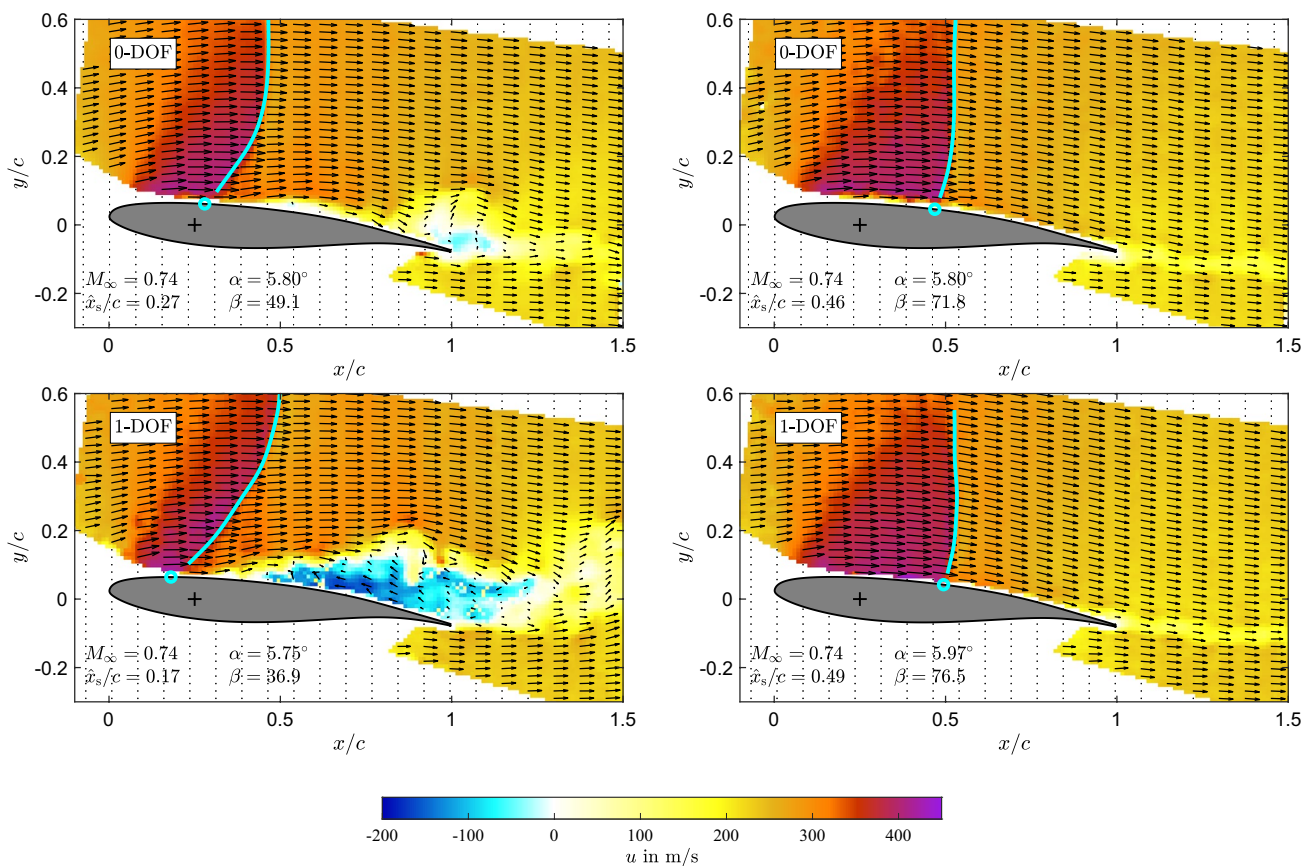
Fig. 4 Examples of instantaneous flow fields with the shock located at an extreme upstream (left) and an extreme downstream location (right) for the case without (top) and with (bottom) pitching degree of freedom. The same Mach number $M_\infty = 0.74$ and mean angle of attack $\overline{\alpha} \approx 5.8°$ were chosen for both cases. The solid lines indicate the detected shock position and the open circles show the extrapolated shock-foot location on the airfoil's surface. In x- and y-directions, every seventh and every second vector is shown, respectively

buffet is not yet fully developed or that natural frequencies in Ref. [21] allow for coupling between structure and flow similar to the 1-DOF cases presented here.

For $M_\infty = 0.77$, the maximum buffet intensity has already been exceeded and the distributions of the shock-foot location look rather similar again. The mean values are shifted further upstream and the level of fluctuation is decreased. This agrees well with the power spectral density shown in Fig. 7.

3.4 Shock dynamics

To determine the dominant frequencies in the shock motion, the power spectral density of the shock-foot location was computed using the method of Ref. [22] with a window length of 1000 samples, 50% window overlap and a Hamming window weighting function. The resulting spectra are shown in Fig. 7. Since the position of the shock foot was determined from the lower part of the detected shock (see Fig. 4), the spectral content of the shock-foot motion is

superimposed by the motion of the shock up to $y/c = 0.2$. For the 0-DOF case, the spectrum shows a dominant peak only for $M_\infty = 0.74$, which is located around 100 Hz. The two lower Mach numbers do not show any dominant frequency, and for $M_\infty = 0.77$, the peak is significantly reduced, broadened and shifted to $f \approx 120$ Hz. While for $M_\infty = 0.70$ and $M_\infty = 0.72$, there is no buffet yet, and the dominant peak for $M_\infty = 0.74$ indicates a pronounced buffet. At $M_\infty = 0.77$, the buffet intensity already decreases again.

The 1-DOF case also shows the strongest peak for $M_\infty = 0.74$. In contrast to the 0-DOF case, however, a similarly strong intensity is detected for $M_\infty = 0.72$ and still a moderate buffet intensity for $M_\infty = 0.77$. This result supports the findings of Refs. [23, 24], according to which the additional degree of freedom can lead to a premature occurrence of buffet. For $M_\infty = 0.74$, the peak is shifted to higher frequencies compared to the 0-DOF case. This suggests that in the coupling of structure and flow, the natural frequency of the structure becomes dominant, as observed for transonic frequency lock-in FLI [25]. However,
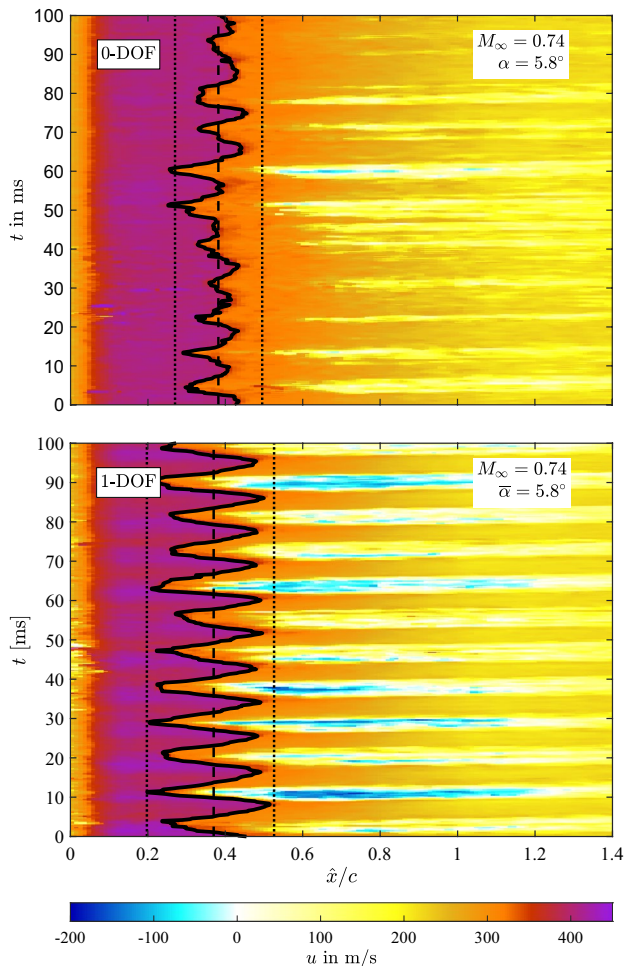
Fig. 5 Time evolution of the horizontal velocity component u for a fixed height of $\hat{y} = 0.1$ above the chord for the case without (top) and with (bottom) pitching degree of freedom. The same Mach number $M_\infty = 0.74$ and mean angle of attack $\overline{\alpha} \approx 5.8°$ were chosen for both cases. The dashed and dotted lines represent the median shock location at this height and the corresponding 95% coverage, respectively. The solid line indicates the shock location

Fig. 6 Histogram of the shock-foot location for different Mach numbers for the case without (top) and with (bottom) pitching degree of freedom

Fig. 7 Power spectral density of the shock-foot location for different Mach numbers for the case without (top) and with (bottom) pitching degree of freedom

the relatively low ratio of structure frequency to buffet frequency (in the 0-DOF case) of 115.5 Hz/98.5 Hz indicates that the coupling is still in transition between the fluid mode and structural mode, as discussed in Refs. [26–28].

Another important difference to the 0-DOF case is that the peaks in the 1-DOF case are much narrower and, therefore, more dominant. This agrees well with the temporal evolution of the shock location, which was significantly more harmonic with pitching degree of freedom (see Fig. 5).

As shown in the histograms in Fig. 6, the shock motion amplitude increases significantly after buffet onset. This causes the shock to move with higher velocity in order to cover a certain distance per cycle. The shock foot's velocity for the different cases was estimated from the PIV vector fields and is illustrated in Fig. 8. For the pre-buffet
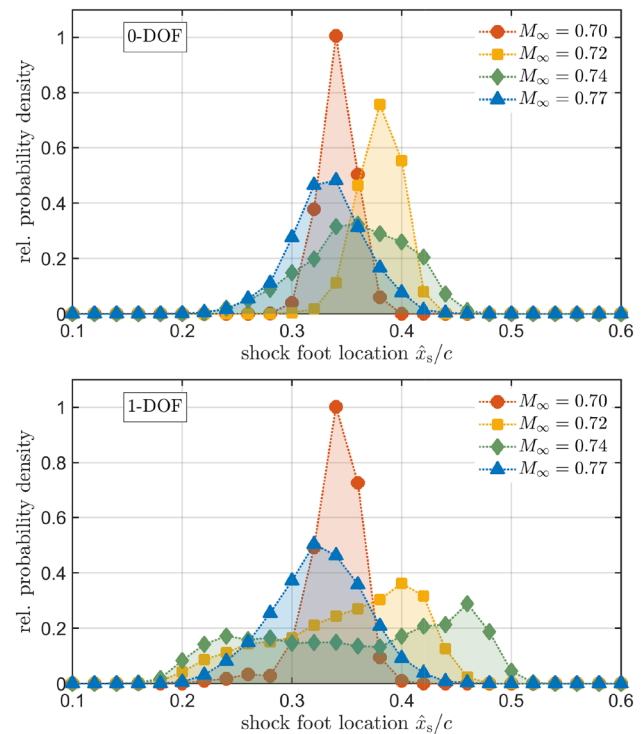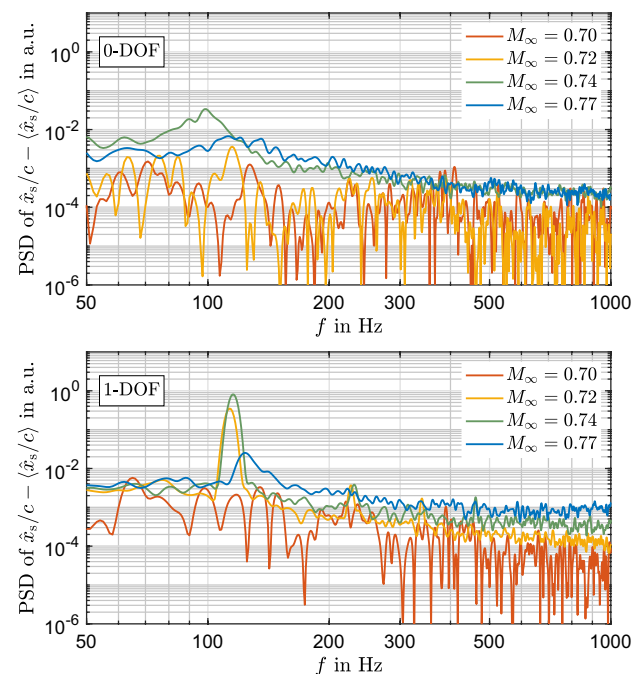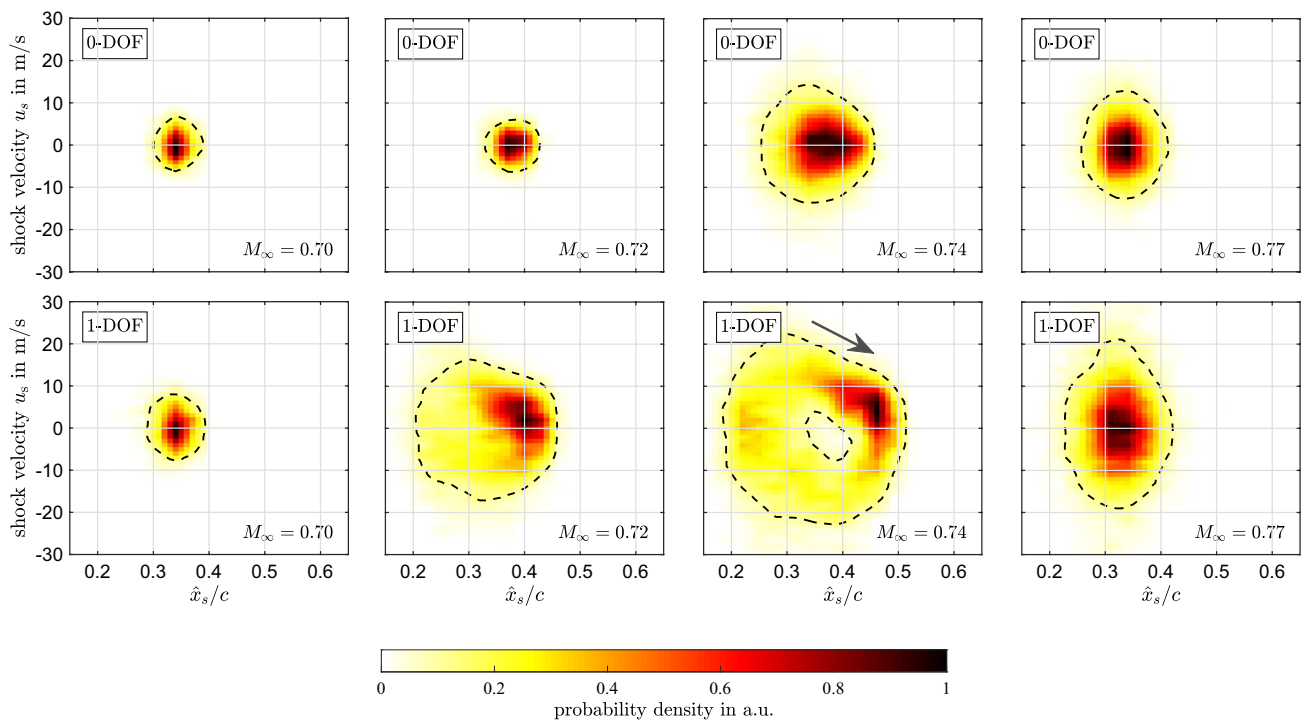
Fig. 8 Joint probability density distribution of shock-foot velocity u_s and shock location $\hat{x}_s$ for the model with (bottom) and without (top) pitching degree of freedom for different Mach numbers. The dashed line indicates the decrease to 10% of the corresponding maximum value

cases, the velocity distribution is symmetric and the velocities are within the range of $u_s = \pm 10$ m/s. When increasing the Mach number, the velocity distributions for the cases with and without pitching degree of freedom differ. For the 0-DOF case, the values of u_s exceed ± 10 m/s and the highest probability is found around zero velocity. This is due to the fact that the shock often changes direction, as can be seen in Fig. 5 in the top row. For the 1-DOF case, buffet starts already at $M_\infty = 0.72$ and for $M_\infty = 0.74$ velocities beyond $u_s = \pm 20$ m/s are reached. It is noticeable that the probability distribution is no longer symmetrical. For $M_\infty = 0.74$, the highest probability is found for a slowly downstream moving shock that is already in the vicinity of its rear turning point. Moreover, the distribution function has an annular shape with a local minimum at $\hat{x}_s/c \approx 0.37$ and $u_s \approx 3$ m/s, rather than a Gaussian shape. From the shape of the distribution, it can be concluded that shock velocity and shock location are highly correlated with each other in this case.

For $M_\infty = 0.77$, the distribution in Fig. 8 returns to a similar version as in the pre-buffet. For the 1-DOF case, the variations of velocity and shock location are slightly larger, but both distribution functions show a similar Gaussian-like shape with a maximum at zero velocity.

3.5 Shock angle analysis

One way to determine the state of the boundary layer is to find the shock angle β, where β is the angle between the model surface and the shock at the shock foot (see Fig 2). Theoretically, β can take values between the Mach angle of the local Mach number and 90°. The larger the shock angle, the stronger the shock and thus the pressure rise across it. However, if a strong shock leads to a separation, the flow direction changes and affects the shock. In the following, the shock angle reduces and the shock weakens. It was shown in Ref. [11] using single-pixel PIV evaluation methods that in the case of an oblique compression shock, separation was always evident, while for shock angles close to 90°, boundary layer thickening was the only detectable feature.

To determine when the flow is detached and when it is attached, the shock angle at the model surface was determined from the PIV results. Figure 9 shows the joint probability density distribution of the shock angle β and the shock location $\hat{x}_s$ for the model with and without pitching degree of freedom for the different Mach numbers.

For the smallest Mach number of $M_\infty = 0.70$, both cases show a narrow and symmetric Gaussian-like distribution with the maximum located at $\beta \approx 75°$. This shock angle results from a slight deflection of the flow due to a sudden
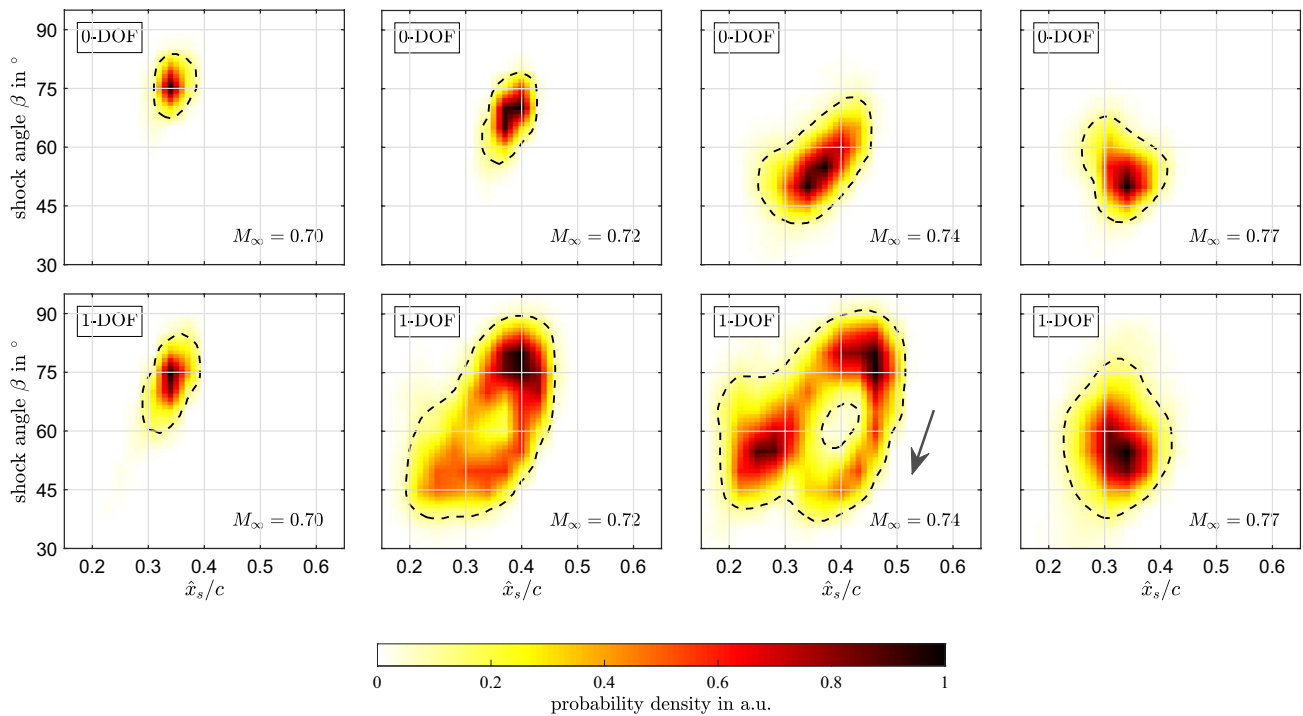
Fig. 9 Joint probability density distribution of shock angle β and shock location $\hat{x}_s$ for the model with (bottom) and without (top) pitching degree of freedom for different Mach numbers. The dashed line indicates the decrease to 10% of the corresponding maximum value

increase in boundary layer thickness downstream of the shock. A flow separation does not occur here, or only very rarely.

For $M_\infty = 0.72$, the distributions broaden significantly. The shock angles are now between 55° and 80° for the 0-DOF case and between 40° and 90° for the 1-DOF case. From this, it can be deduced that the shock causes moderate deflection of the streamlines temporarily in the 0-DOF case and even strong deflection in the 1-DOF case. The stronger the streamline deflection, the more likely it is to result from flow separation.

For $M_\infty = 0.74$, the shock angle distribution broadens further in the 0-DOF case and shifts towards smaller shock angles. This increases the probability of boundary layer separation during the buffet cycle. In the 1-DOF case, the distribution forms again an annular structure with a local minimum in the center. At the most upstream position, the shock is at a lower angle (highest probability for about 55°) and as it moves downstream, the angle increases continuously, reaching values up to about 90°. In the vicinity of the rear turning point, flow separation occurs, during which the shock angle is strongly reduced while the shock then moves upstream again. In contrast to the 0-DOF case, it is very likely that the flow is separated and also attached during each buffet cycle.

For $M_\infty = 0.77$, both distributions become more symmetric again and shift to lower shock angles compared to the

pre-buffet cases. The highest probability is around $\beta = 50°$ and $\beta = 55°$ for the 0-DOF case and the 1-DOF case, respectively. It can be concluded that the flow is mainly separated for this Mach number.

3.6 Fluid–structure coupling

If the buffet frequency is close to the pitching frequency, a synchronized motion of the shock and the airfoil is possible. Figure 10 shows the probability distribution of the shock-foot location and the angle of attack for the tested Mach numbers. It is clear from the figure that for $M_\infty = 0.72$ and 0.74, both quantities are directly coupled. For $M_\infty = 0.70$ and 0.77, no coupled motion is observed. For $M_\infty = 0.74$, the shape of the probability distribution has an annular structure similar to the distributions of shock angle and shock velocity. When the shock foot is at its most downstream (or upstream) location, the angle of attack is close to its maximum (or minimum) and will reach it shortly after the downstream (or upstream) turning point of the shock. Thus, the change in α and $\hat{x}_s$ are highly correlated and follow a certain phase delay.

The correlation coefficient and the phase difference were evaluated from the following correlation function:

$$R_{\alpha,\hat{x}_s}(\tau) = \frac{\sum_{n=1}^{N} \alpha'(t-\tau) \cdot \hat{x}_s'(t)}{N \cdot \sigma_\alpha \cdot \sigma_{\hat{x}_s}} \tag{1}$$
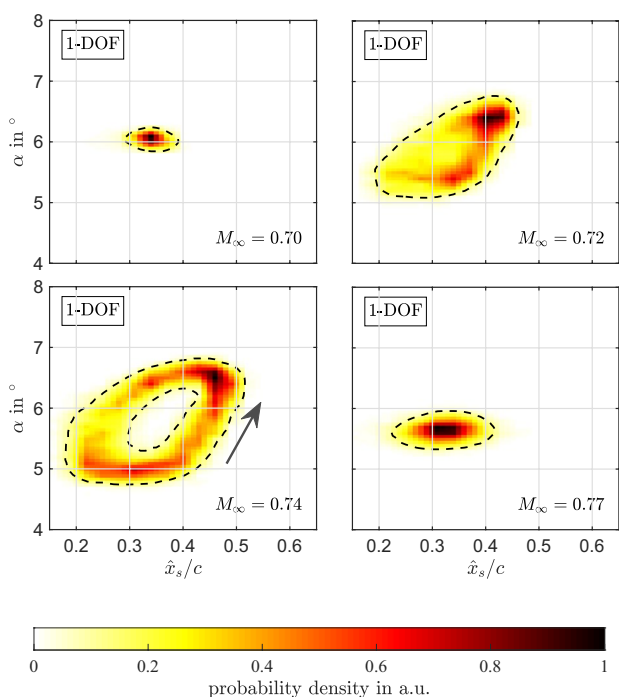
Fig. 10 Joint probability density distribution of the angle of attack α and the shock-foot location $\hat{x}_s$ for the model with pitching degree of freedom for different Mach numbers. The dashed line indicates the decrease to 10% of the corresponding maximum value

where α', $\hat{x}_s'$, σ_α, and $\sigma_{\hat{x}_s}$ are the fluctuation values about the mean and the standard deviations of the angle of attack and the shock location, respectively. The time shift τ is used to analyze the temporal evolution of the correlation function.

The correlation value is shown in Fig. 11 as a function of τ for the different Mach numbers. The figure shows very good correlation for $M_\infty = 0.72$ and 0.74 with a delay of $\tau = 1.10$ ms and 1.42 ms, which corresponds to 12% and 17% of the buffet period. The cases with $M_\infty = 0.70$ and 0.77
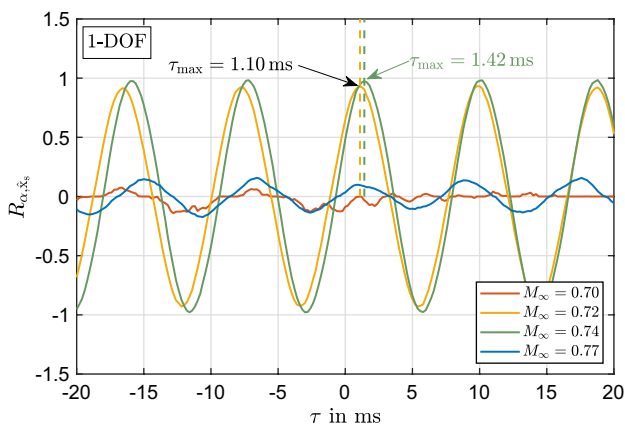
show a low correlation as expected from the probability distribution of α and x_s in Fig. 10.

The analysis at shock positions further from the model surface (at larger $\hat{y}$) instead of the shock foot, exhibits in different delays. Figure 12 illustrates how the time delay changes with the height above chord. For both Mach numbers, τ_{max} decreases continuously with increasing height $\hat{y}$. Thus, the shock foot is always slightly ahead of the model motion in the buffet cycle, while the shock oscillates in phase with α at a certain height (at $\hat{y}/c \approx 0.27$ for $M_\infty = 0.72$, and at $\hat{y}/c \approx 0.47$ for $M_\infty = 0.74$) and lags behind at even larger $\hat{y}$. Furthermore, from the time delay in the correlation, it can be concluded that the shock motion is controlled by events at the shock foot. This is in contradiction with the modification of Ref. [29] to the shock-buffet model of Ref. [5], where the upper end of the shock wave is considered the main interaction region for sound waves starting from the trailing edge. In Ref. [29], it is stated that small deviations of the shock in its upper region, will cause the whole shock to react to these changes. The finding from Fig. 12, however, show that the movement of the upper shock part is only a reaction to the movement of the lower part for the here investigated case. Based on the movement of the shock over time, it can also be concluded from Refs. [2, 3, 21] that the shock motion is initiated at the shock foot.

4 Summary and conclusions

High repetition rate PIV measurements of the transonic flow over an OAT15A airfoil model with an optional pitching degree of freedom were performed at the trisonic wind tunnel Munich. A Mach number variation between $M_\infty = 0.70$ und 0.77 allowed for investigating the flow in pre-buffet, fully developed buffet, and off-setting buffet conditions. The comparison between the cases with and without pitching
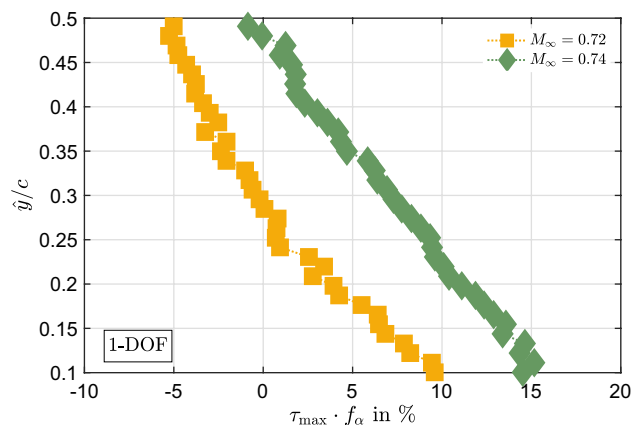

Fig. 11 Correlation of angle of attack α and shock-foot location $\hat{x}_s$ as a function of the delay time τ according to Eq. (1)

Fig. 12 Time delay τ_{max} between motion of angle of attack and shock location at different shock heights $\hat{y}$ normalized by the cycle time $1/f_\alpha$

degree of freedom revealed significant differences. For the investigated test cases, the pitching degree of freedom significantly enhanced the dynamics of the flow field compared to a model with zero degree of freedom. In the 1-DOF case, the shock oscillates over a larger streamwise distance and its motion is highly periodic. Furthermore, the boundary layer state alternates between attached and detached, and the shock angle changes between (almost) straight shock and clearly oblique shock for each cycle.

In the 0-DOF case, on the other hand, the shock motion appears less harmonic (see Fig. 5), resulting in a significantly broadened peak in the spectrum (see Fig. 7). In addition, the shock angle shows less changes during the buffet cycle (see Fig. 9). While the case with the most pronounced buffet behavior for the given conditions for this model was considered here, it is still possible that buffet is not fully developed. There could be other effects that influence or shift the conditions for which fully developed buffet occurs. This could be related to the relatively small aspect ratio, to the boundary layer tripping or to wind tunnel wall effects, as discussed in Refs. [14, 18].

In fully developed buffet flow conditions, a coupled periodic change of the angle of attack and the shock position was observed for the 1-DOF case. A correlation of both quantities showed a delay of 12% (for $M_\infty = 0.72$) and 17% (for $M_\infty = 0.74$), where the angle of attack reaches its maximum later than the shock-foot location. The correlation with different shock heights showed that the shock motion is led by the shock foot.

It can be concluded that the pitching degree of freedom significantly affects the flow field in terms of periodicity and amplitude of the shock motion. This is an important fact that must be taken into account when developing aeronautical components for use in transonic flow conditions.

Data availability No additional data is provided.

Declarations

Conflict of interest The authors have no relevant financial or non-financial interests to disclose.

References

1. Crouch, J.D., Garbaruk, A., Magidov, D., Travin, A.: Origin of transonic buffet on aerofoils. J. Fluid Mech. **628**, 357 (2009). https://doi.org/10.1017/S0022112009006673

2. Iovnovich, M., Raveh, D.E.: Reynolds-averaged Navier–Stokes study of the Shock–Buffet instability mechanism. AIAA J. **50**(4), 880 (2012). https://doi.org/10.2514/1.J051329

3. Jacquin, L., Molton, P., Deck, S., Maury, B., Soulevant, D.: Experimental study of shock oscillation over a transonic supercritical profile. AIAA J. **47**(9), 1985 (2009). https://doi.org/10.2514/1.30190

4. Giannelis, N.F., Vio, G.A., Levinski, O.: A review of recent developments in the understanding of transonic shock buffet. Prog. Aerosp. Sci. **92**, 39 (2017). https://doi.org/10.1016/j.paerosci.2017.05.004

5. Lee, B.H.K.: Self-sustained shock oscillations on airfoils at transonic speeds. Prog. Aerosp. Sci. **37**(2), 147 (2001). https://doi.org/10.1016/S0376-0421(01)00003-3

6. McDevitt, J.B., Okuno, A.F.: Static and dynamic pressure measurements on a NACA 0012 airfoil in the Ames high Reynolds number facility. Tech. rep. (1985)

7. Tijdeman, H.: Investigations of the transonic flow around oscillating airfoils. Ph.D. thesis, TU Delft (1977)

8. Gao, C., Zhang, W.: Transonic aeroelasticity: a new perspective from the fluid mode. Prog. Aerosp. Sci. **113**, 100596 (2020). https://doi.org/10.1016/j.paerosci.2019.100596

9. Nitzsche, J., Ringel, L.M., Kaiser, C., Hennings, H.: In: IFASD 2019 International Forum on Aeroelasticity and Structural Dynamics. https://elib.dlr.de/127989/ (2019). Accessed 13 June 2019

10. Kokmanian, K., Scharnowski, S., Schäfer, C., Accorinti, A., Baur, T., Kähler, C.J.: Investigating the flow field dynamics of transonic shock buffet using particle image velocimetry. Exp. Fluids **63**(9), 149 (2022). https://doi.org/10.1007/s00348-022-03499-2

11. Scharnowski, S., Kokmanian, K., Schäfer, C., Baur, T., Accorinti, A., Kähler, C.J.: Shock-buffet analysis on a supercritical airfoil with a pitching degree of freedom. Exp. Fluids **63**(6), 93 (2022). https://doi.org/10.1007/s00348-022-03427-4

12. Scharnowski, S., Bross, M., Kähler, C.J.: Accurate turbulence level estimations using PIV/PTV. Exp. Fluids **60**(1), 1 (2019). https://doi.org/10.1007/s00348-018-2646-5

13. Scheitle, H., Wagner, S.: Influences of wind tunnel parameters on airfoil characteristics at high subsonic speeds. Exp. Fluids **12**(1–2), 90 (1991). https://doi.org/10.1007/BF00226571

14. Accorinti, A., Baur, T., Scharnowski, S., Kähler, C.J.: Experimental investigation of transonic shock buffet on an OAT15A profile. AIAA J. (2022). https://doi.org/10.2514/1.J061135

15. Korthäuer, T., Accorinti, A., Scharnowski, S., Kähler, C.J.: Effect of Mach number and pitching eigenfrequency on transonic buffet onset. AIAA J. **61**(1), 112 (2023). https://doi.org/10.2514/1.J061915

16. Korthäuer, T., Accorinti, A., Scharnowski, S., Kähler, C.J.: (2023) Experimental investigation of transonic buffeting, frequency lock-in and their dependence on structural characteristics. J. Fluids

Struct. **122**, 103975 (2023). https://doi.org/10.1016/j.jfluidstructs.2023.103975

17. Bross, M., Scharnowski, S., Kähler, C.J.: Large-scale coherent structures in compressible turbulent boundary layers. J. Fluid Mech. **911**, A2 (2021). https://doi.org/10.1017/jfm.2020.993

18. Accorinti, A., Baur, T., Scharnowski, S., Kähler, C.J.: Characterization of transonic shock buffet over the span of an OAT15A profile. Exp. Fluids **64**, 61 (2023). https://doi.org/10.1007/s00348-023-03604-z

19. Scharnowski, S., Kähler, C.J.: Particle image velocimetry—classical operating rules from today's perspective. Opt. Lasers Eng. (2020). https://doi.org/10.1016/j.optlaseng.2020.106185

20. Westerweel, J., Scarano, F.: Universal outlier detection for PIV data. Exp. Fluids **39**, 1096 (2005). https://doi.org/10.1007/s00348-005-0016-6

21. D'Aguanno, A., Schrijer, F.F.J., van Oudheusden, B.W.: Experimental investigation of the transonic buffet cycle on a supercritical airfoil. Exp. Fluids **62**(10), 214 (2021). https://doi.org/10.1007/s00348-021-03319-z

22. Welch, P.D.: The use of fast fourier transform for the estimation of power spectra: a method based on time averaging over short, modified periodograms. IEEE Trans. Audio Electroacoust. (1967). https://doi.org/10.1109/TAU.1967.1161901

23. Nitzsche, J.: In: IFASD 2009—International Forum on Aeroelasticity and Structural Dynamics, Seattle, WA, USA. https://elib.dlr.de/61964/ (2009)

24. Gao, C., Zhang, W., Ye, Z.: Reduction of transonic buffet onset for a wing with activated elasticity. Aerosp. Sci. Technol. **77**, 670 (2018). https://doi.org/10.1016/j.ast.2018.03.047

25. Raveh, D.E., Dowell, E.H.: Frequency lock-in phenomenon for oscillating airfoils in buffeting flows. J. Fluids Struct. **27**(1), 89 (2011). https://doi.org/10.1016/j.jfluidstructs.2010.10.001

26. Gao, C., Zhang, W., Ye, Z.: A new viewpoint on the mechanism of transonic single-degree-of-freedom flutter. Aerosp. Sci. Technol. **52**, 144 (2016). https://doi.org/10.1016/j.ast.2016.02.029

27. Gao, C., Zhang, W., Li, X., Liu, Y., Quan, J., Ye, Z., Jiang, Y.: Mechanism of frequency lock-in in transonic buffeting flow. J. Fluid Mech. **818**, 528–561 (2017). https://doi.org/10.1017/jfm.2017.120

28. Giannelis, N.F., Vio, G.A., Dimitriadis, G.: In: Proceedings of the 27th International Conference on Noise and Vibration Engineering, pp 457–470. Leuven, Belgium (2016)

29. Hartmann, A., Feldhusen, A., Schröder, W.: On the interaction of shock waves and sound waves in transonic buffet flow. Phys. Fluids **25**(2), 026101 (2013). https://doi.org/10.1063/1.4791603